

MULTI-WAVELENGTH OBSERVATIONS OF A NEW REDBACK MILLISECOND PULSAR 4FGL J1910.7–5320

KA-YUI AU,¹ JAY STRADER,² SAMUEL J. SWIHART,³ LUPIN C. C. LIN,¹ ALBERT K. H. KONG,⁴ JUMPEI TAKATA,⁵
CHUNG-YUE HUI,⁶ TERESA PANURACH,² ISABELLA MOLINA,² ELIAS AYDI,² KIRILL SOKOLOVSKY,² AND KWAN-LOK LI¹

¹*Department of Physics, National Cheng Kung University
No. 1 University Road, Tainan City 70101, TAIWAN*

²*Department of Physics and Astronomy, Michigan State University, East Lansing, MI 48824, USA*

³*National Research Council Research Associate, National Academy of Sciences, Washington, DC 20001, USA
resident at Naval Research Laboratory, Washington, DC 20375, USA*

⁴*Institute of Astronomy, National Tsing Hua University
Hsinchu 30013, Taiwan*

⁵*School of Physics, Huazhong University of Science and Technology
Wuhan 430074, People's Republic of China*

⁶*Department of Astronomy and Space Science, Chungnam National University
Daejeon 34134, Republic of Korea*

ABSTRACT

We present the study of multi-wavelength observations of an unidentified *Fermi* Large Area Telescope (LAT) source, 4FGL J1910.7–5320, a new candidate redback millisecond pulsar binary. In the 4FGL 95% error region of 4FGL J1910.7–5320, we find a possible binary with a 8.36-hr orbital period from the Catalina Real-Time Transient Survey (CRTS), confirmed by optical spectroscopy using the SOAR telescope. This optical source was recently independently discovered as a redback pulsar by the TRAPUM project, confirming our prediction. We fit the optical spectral energy distributions of 4FGL J1910.7–5320 with a blackbody model, inferring a maximum distance of 4.1 kpc by assuming that the companion fills its Roche-lobe with a radius of $R = 0.7 R_{\odot}$. Using a 12.6 ks *Chandra* X-ray observation, we identified an X-ray counterpart for 4FGL J1910.7–5320, with a spectrum that can be described by an absorbed power-law with a photon index of 1.0 ± 0.4 . The spectrally hard X-ray emission shows tentative evidence for orbital variability. Using more than 12 years of *Fermi*-LAT data, we refined the position of the γ -ray source, and the optical candidate still lies within the 68% positional error circle. In addition to 4FGL J1910.7–5320, we find a variable optical source with a periodic signal of 4.28-hr inside the 4FGL catalog 95% error region of another unidentified *Fermi* source, 4FGL J2029.5–4237. However, the γ -ray source does not have a significant X-ray counterpart in a 11.7 ks *Chandra* observation, with a $3\text{-}\sigma$ flux upper limit of $2.4 \times 10^{-14} \text{ erg cm}^{-2} \text{ s}^{-1}$ (0.3–7 keV). Moreover, the optical source is outside our updated *Fermi*-LAT 95% error circle. These observational facts all suggest that this new redback millisecond pulsar powers the gamma-ray source 4FGL J1910.7–5320 while 4FGL J2029.5–4237 is unlikely the γ -ray counterpart to the 4.28-hr variable.

Keywords: Millisecond pulsars (1062), Gamma-ray sources (633), Compact binary stars (283)

1. INTRODUCTION

Millisecond pulsars (MSPs) are neutron stars with a very short spin period on the order of one thousandth

of a second. One widely accepted explanation, known as the recycling scenario, is that MSPs were in binaries with donor stars and the accretion from a companion in a binary system continuously transfers the angular momentum to the pulsar (Alpar et al. 1982, and some MSPs still remain in binaries after the recycling process). If the binaries started the recycling phase at long orbital periods, then the MSPs will be formed with a

complex evolution dynamics. In these cases, the donors are far away from the pulsars, it did not fill the Roche lobes during the process until it became a (sub)giant, which typically leads to an MSP-He White Dwarf (WD) system (Tauris 2011; Hui et al. 2018). For the low-mass X-ray binaries (LMXBs) that started the recycling process in tighter orbits, special subclasses of pulsar binaries can be formed: reback and black widow MSPs.

The two classes have compact orbits, and hence, short periods (≤ 1 day) with very low-mass companions ($M_C \gtrsim 0.1 M_\odot$ for rebacks and $< 0.1 M_\odot$ for black widows; Roberts 2011; Chen et al. 2013). They are called rebacks and black widows in analogy to the conduct of real spiders: the female reback and black widow spider cannibalizes their companion after copulation, just like the central neutron stars create energetic pulsar winds and high-power radiation fields, which ablate the nearby companions. This scenario could explain how isolated MSPs are formed (Van den Heuvel & Van Paradijs 1988). In recent years, some reback MSPs, PSR J1227-4853 (Roy et al. 2015), PSR J1023+0038 (Archibald et al. 2009; Patruno et al. 2013; Stappers et al. 2014), and M28I (Papitto et al. 2013), showed a transition between the LMXB state and the radio pulsar state, providing strong evidence supporting the recycling scenario of the MSPs formation (Alpar et al. 1982).

Before the launch of the *Fermi* Large Area Telescope (LAT), discovering reback and black widow MSPs was challenging because the material blown off from the companion by the high-power pulsar wind/radiation can hide the radio emission of the pulsar. Therefore, it is difficult to find the MSP radio pulsations in blind all-sky radio surveys. However, the GeV γ -ray emission is not affected by the obscuring material, making LAT a great tool to discover reback and black widow MSP candidates with follow-up observations in other wavelengths, given that many reback/black widow MSPs have γ -ray emission (Abdo et al. 2013; Swihart et al. 2022). Nowadays, it is also possible to find MSP binaries by using optical data from all-sky surveys (ZTF and *Gaia*; *Gaia* Collaboration et al. 2016; Bellm et al. 2018; Burdge et al. 2022).

LAT, the main instrument on the *Fermi Gamma-ray Space Telescope*, is an imaging telescope for high-energy γ -rays in the range of 100 MeV–300 GeV (Atwood et al. 2009). Using 12 years of LAT data, the *Fermi*-LAT science team made the *Fermi*-LAT Fourth Source Catalog Data Release 3 (4FGL-DR3; Abdollahi et al. 2022) to list the known properties of all the detected point-like and extended γ -ray sources of *Fermi*-LAT. 4FGL (Abdollahi et al. 2020; the first data release) and 4FGL-DR3

share the same data analysis method and model for the Galactic interstellar emission. One of the major differences between them is that 4FGL-DR3 used four more years than 4FGL, and so the inferred parameters of the 4FGL-DR3 γ -ray sources are generally more accurate.

In this paper, two pulsar-like unassociated *Fermi* sources, 4FGL J1910.7–5320 and 4FGL J2029.5–4237, were investigated. For 4FGL J1910.7–5320, we present the multi-wavelength observations, including the data from *Fermi*-LAT, *Chandra X-ray observatory*, the Southern Astrophysical Research (SOAR) telescope, and the Catalina survey, strongly suggesting that it is a reback MSP candidate. In addition, the Transients and Pulsars with MeerKAT (TRAPUM) team has independently found the radio pulsations associated with 4FGL J1910.7–5320, which is in line with our result. We also present the γ -ray, X-ray, and optical analyses of 4FGL J2029.5–4237. However, we find no evidence that this second unassociated GeV source is a pulsar binary system.

2. SEARCHING FOR SPIDER MSP CANDIDATES WITH 4FGL-DR3/CRTS

Since the first catalog release of *Fermi*-LAT, there have been numerous attempts to expand the reback and black widow MSP population by searching the LAT catalog for new pulsar systems (e.g., Kong et al. 2014; Hui et al. 2015; Li et al. 2016; Strader et al. 2016). These searches are based on the well-known fact that most MSPs have (i) stable γ -ray light curves on a monthly time-scale, and (ii) curved γ -ray spectra rather than a simple power-law. In this project, we did not use the spectral and timing properties of the γ -ray sources for picking up candidates. We cross-checked the 4FGL-DR3 and the Catalina Surveys Southern periodic variable star catalogs of the Catalina Real-Time Transient Surveys (CRTS; Drake et al. 2009, 2017; Abdollahi et al. 2022) and selected possible γ -ray emitting compact binaries with the following criteria.

- The 4FGL-DR3 γ -ray sources must be “unassociated sources” with detection significances higher than 5σ and high Galactic latitudes (i.e., $|b| > 5^\circ$).
- For all the selected 4FGL-DR3 sources, the semi-major axes of the 95% error circles must be smaller than 0.1° to minimize the contamination (i.e. unrelated CRTS sources).
- The periods of the selected CRTS variables must be shorter than 24 hours.
- The selected CRTS sources must be fainter than 15 mag. Reback and black widow systems are generally fainter than the threshold, although there

are counterexamples, e.g., 3FGL J0212.1+5320 (Li et al. 2016). If a redback/black widow has an apparent magnitude of < 15 mag, it is probably a very nearby pulsar system (i.e. ≤ 1 kpc), and might have been discovered by the pulsar surveys.

Ten candidates were selected using the above method. We then further cross-checked the candidates with the SIMBAD¹ database, and found that 6 of them are RR Lyrae variable and 1 of them is a known redback MSP candidate, 3FGL J0954.8–3948 (Li et al. 2018). We examined visually the CRTS light curves of the rest of the candidates. One of them is an Algol type variable, which has two obvious eclipse dips seen in the light curve. The other two, 4FGL J1910.7–5320 and 4FGL J2029.5–4237, show sinusoidal-like modulations, possibly caused by “pulsar heating” and/or ellipsoidal variation, if they are pulsar systems (Romani & Sanchez 2016; Draghis et al. 2019; Hui & Li 2019; Yap et al. 2019). We therefore started a multi-wavelength follow-up campaign for the two systems.

3. 4FGL J1910.7–5320

In the following subsections, we will focus on the results of the multi-wavelength observations of 4FGL J1910.7–5320.

3.1. CRTS Surveys Data And Vizier Photometry Viewer

We downloaded and re-analyzed the optical data of 4FGL J1910.7–5320 from the CRTS (Drake et al. 2009) to confirm, and perhaps improve, the period from the CRTS catalog. The phased light curves were also investigated to see if they are consistent with that of a pulsar binary. In addition, the spectral energy distribution (SED) in the optical band obtained from the VizierR Photometry viewer² was used to estimate the color temperature of the source as well as the distance to the system.

The CRTS observations were taken from 2005 Aug 01 to 2013 Jun 21, and the variable source is located at R.A.(J2000) = $19^{\text{h}}10^{\text{m}}49^{\text{s}}.12$, Decl.(J2000) = $-53^{\circ}20'57''.1$. We fit the CRTS data with a sinusoidal function and found that the period is 0.3484776(10) days (roughly 8.36 hours) with a mean magnitude of 19.08 ± 0.01 mag and an amplitude of 0.54 ± 0.02 mag. We note that the period in the CRTS catalog is 0.697 days (twice our best-fit period; Drake et al. 2017), and at this period, the folded light curve shows a double-peaks

¹ <http://simbad.cds.unistra.fr/simbad/>

² <http://vizier.unistra.fr/vizier/sed/>

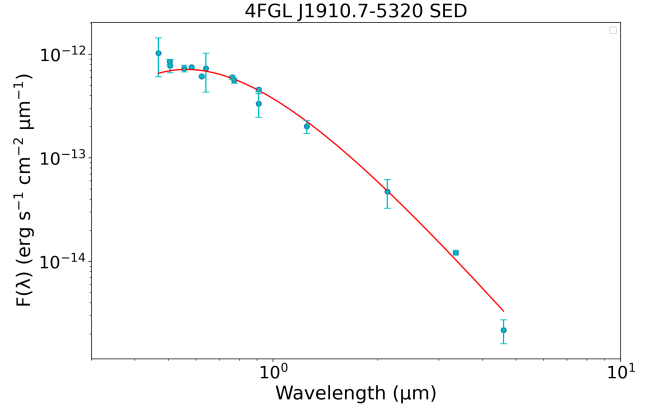


Figure 1. Optical spectral energy distribution (SED) of 4FGL J1910.7–5320 with extinction correction. The red line is the best-fit blackbody model.

feature. Given that the 0.697-day period is inconsistent with the SOAR observations (see §3.2), we conclude that the 8.36-hour period is the real one. More detailed investigations will be discussed in the next subsection.

For the SED, we included data from *Gaia* (Gaia Collaboration et al. 2016; Brown et al. 2018; Gaia Collaboration 2020), *GALEX* (Bianchi et al. 2011), POSS (Lasker et al. 2008), VISTA (McMahon et al. 2013) and *WISE* (Marocco et al. 2021), and corrected for the absorption using the extinction function from Cardelli et al. (1989) with the total absorption in magnitudes of $A_v = 0.1857$ mag and the ratio of total to selective absorption of $R_v = 3.1$ (Schlegel et al. 1998). Then we used a blackbody radiation model to fit the SED data (Figure 1). The best-fit color temperature is $T = 5154 \pm 164$ K, and the inferred distance is $D = 5.8_{-0.4}^{+0.5}$ (R/R_\odot) kpc where R is the companion radius.

Assuming that the companion nearly fills up the Roche-lobe, we used the approximate formula from Eggleton (1983), which is,

$$R = a \times \frac{0.49q^{2/3}}{0.6q^{2/3} + \ln(1 + q^{1/3})} \quad (1)$$

where $q = M_C/M_{MSP}$ (M_C : Mass of companion; M_{MSP} : Mass of MSP) and a is the distance between the binary members, to calculate the Roche-lobe radius. By assuming the masses of the MSP and the companion are 1.4 and $0.4 M_\odot$, respectively, and using Kepler’s Third Law to calculate a , we find $R \lesssim 0.7R_\odot$, and hence, $D \lesssim 4.1$ kpc. If we assumed the companion size is similar to that of a black widow (i.e., $M_C = 0.03M_\odot$), then $R \lesssim 0.3R_\odot$ and $D \lesssim 1.8$ kpc.

Nevertheless, the SED data employed were not obtained simultaneously while the optical source is

strongly variable. To check whether the effect is huge, we tried to find the blackbody model parameters using only the VISTA J- and K-band data (McMahon et al. 2013), which were taken nearly simultaneously. Similar to our original results, the parameters are $T = 4550$ K, $D = 5.2 (R/R_{\odot})$ kpc. The distance is $D \lesssim 3.6$ kpc by assuming the system is redback-like, i.e., $R \lesssim 0.7R_{\odot}$.

We also searched the *Gaia* Catalog DR3 (Gaia Collaboration 2020; Moss et al. 2022) for further distance information, but the parallax is not well constrained (Bailer-Jones et al. 2021).

3.2. SOAR Spectroscopy

We obtained optical spectroscopy of the candidate counterpart to 4FGL J1910.7–5320 using the Goodman Spectrograph (Clemens et al. 2004) on the SOAR telescope over six nights from 2022 Apr 10 to 2022 Jun 10, typically taking multiple spectra per night. For all spectra we used a $1''.2$ slit and a 400 lmm^{-1} grating covering a wavelength range of $\sim 3950\text{--}7850 \text{ \AA}$, giving a resolution of about 7.3 \AA for full-width at half-maximum. The spectra were reduced and optimally extracted using standard routines in IRAF (Tody 1986). We obtained 20 total usable spectra in this setup (Table 1).

The spectra generally appear consistent with a late G/early K type star (Figure 2). The most prominent absorption lines are *Mgb* and Na D, along with several Fe lines. $\text{H}\alpha$ and $\text{H}\beta$ are present in absorption in some of the SOAR spectra, while in others $\text{H}\alpha$ is weak or absent. There are no clear emission lines in any spectra.

We derived barycentric radial velocities (RVs) through cross-correlation with a high signal-to-noise template spectrum in the region of *Mgb*. We fit a circular Keplerian model to the velocities. As the fitting spectroscopic period is consistent with the photometric period, we fix it to the latter as the time span of the photometry is much longer than that of the spectroscopy.

The model parameters of the fitting model are $K_{2,obs} = 219 \pm 14 \text{ km s}^{-1}$, $\gamma = -17 \pm 12 \text{ km s}^{-1}$, and $T_0 = \text{BJD } 2459700.8091(41)$, where $K_{2,obs}$ is semi-amplitude, γ is systemic velocity, and T_0 is the ascending node of the pulsar in Barycentric Julian Date (BJD). This fit has a $\chi^2/\text{degree of freedom (d.o.f.)}$ of $38/17$ and a root-mean-square (r.m.s.) of 30.9 km s^{-1} , suggesting an imperfect fit. Two of the most negative velocity measurements seem to be unexpected outliers and could have underestimated uncertainties; if these points were excluded, the quality of the fit would be substantially improved. But we have no specific justification for such a change, so we retain the full dataset, and acknowledge this is a preliminary characterization that could be improved with more data in the future.

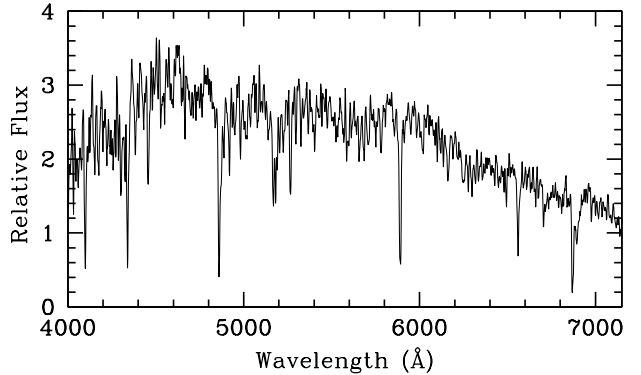


Figure 2. A sample spectrum of the optical counterpart to 4FGL J1910.7–5320 from 2022 Apr 11. A relative flux calibration has been applied, and the spectrum smoothed with a 3-pixel boxcar for display. Prominent metal and Balmer absorption lines are apparent, as described in §3.2.

We re-fit both the CRTS and SOAR data assuming a pulsar heating scenario (i.e., the CRTS light curve leads the SOAR RV curve by $\frac{\pi}{2}$). The best-fit parameters are an orbital period of $0.34847592(21)$ days, a mean CRTS magnitude of 19.015 ± 0.018 mag, a CRTS amplitude of 0.506 ± 0.029 mag, $K_{2,obs} = 218 \pm 8 \text{ km s}^{-1}$, $\gamma = -17 \pm 6 \text{ km s}^{-1}$ and the phase zero at BJD 2453584.0121(31). We use the best-fit parameters of $P = 0.34847592$ days and phase zero at BJD 2453584.0121 to fold both the CRTS light and the RV curves, which are plotted in Figure 3 and 4, respectively.

It is clear that we have incomplete phase coverage of the source in Figure 3, missing data around $\phi = 0.25$ when the secondary is the faintest. This is not solely chance, but reflects the observational biases induced by the observational window available. Nonetheless, the main orbital parameters are relatively well-constrained.

Because of irradiation, $K_{2,obs}$ is not necessarily the same as the center of mass K_2 , though no extreme changes are observed in the optical spectra at different phases. The observed mass function implied by the optical spectroscopy is $f = 0.37 \pm 0.02 M_{\odot}$, which is a typical value for a spider binary. Even accounting for the uncertainty in the true K_2 value, this mass function (which approximately represents the minimum mass of the primary) implies that an edge-on binary inclination for a neutron star is ruled out, and instead an intermediate inclination is more likely.

3.3. Chandra X-ray Analysis

4FGL J1910.7–5320 was observed with *Chandra* (Weisskopf et al. 2002) for 12.6 ksec on 2019 Nov 20, and we used the *Chandra* data to check whether the CRTS source has an X-ray counterpart. If so, the X-ray data can constrain the X-ray spectral shape and X-ray

Table 1.

Radial Velocities of 4FGL J1910.7–5320 from SOAR		
BJD (days)	Radial Vel. (km s ⁻¹)	Unc. (km s ⁻¹)
2459679.82228114	-46.4	23.6
2459679.84012259	-138.8	27.6
2459679.85806185	-171.1	24.2
2459680.82744858	94.5	27.0
2459680.84495725	66.9	31.4
2459680.86457697	-19.9	26.5
2459700.80192541	-193.2	19.9
2459700.81948426	-214.2	16.7
2459700.83923644	-191.6	18.9
2459722.66462979	15.0	23.9
2459722.68212232	-37.5	25.2
2459724.84289214	-215.2	27.0
2459724.86042189	-284.8	23.3
2459724.88435799	-237.7	33.6
2459740.69388734	220.7	22.6
2459740.71174963	175.3	24.2
2459740.80735656	-29.4	23.8
2459740.82483399	-174.2	20.1
2459740.88603764	-192.1	22.4
2459740.90351553	-287.8	21.1

variability for the putative X-ray counterpart to 4FGL J1910.7–5320.

We used CIAO (version 4.13; Fruscione et al. 2006) to extract the source and background spectra from the *Chandra* data. We made an auxiliary response file (ARF; for both source and background) which is an effective area calibration file where we also applied an energy-dependent point-source aperture correction. We generated a response matrix file (RMF) to map between the properties of the incoming photons and the electronic signals obtained from the detector. After performing a spectral binning with at least 20 counts per bin, we used XSPEC³ (version 12.12.0; Arnaud 1996) from HEASARC to measure the hydrogen column density (which will be a fixed parameter in our spectral model) and the photon index of the X-ray source assuming an absorbed power-law model. We also used the `dmextract` task to generate the light curve with a 2'' radius circular region and 2000 s bin time. Barycentric corrections were performed using `axbary`. In Figure 3, we folded the X-ray light curve using the optical period of $P = 0.34847592$ days.

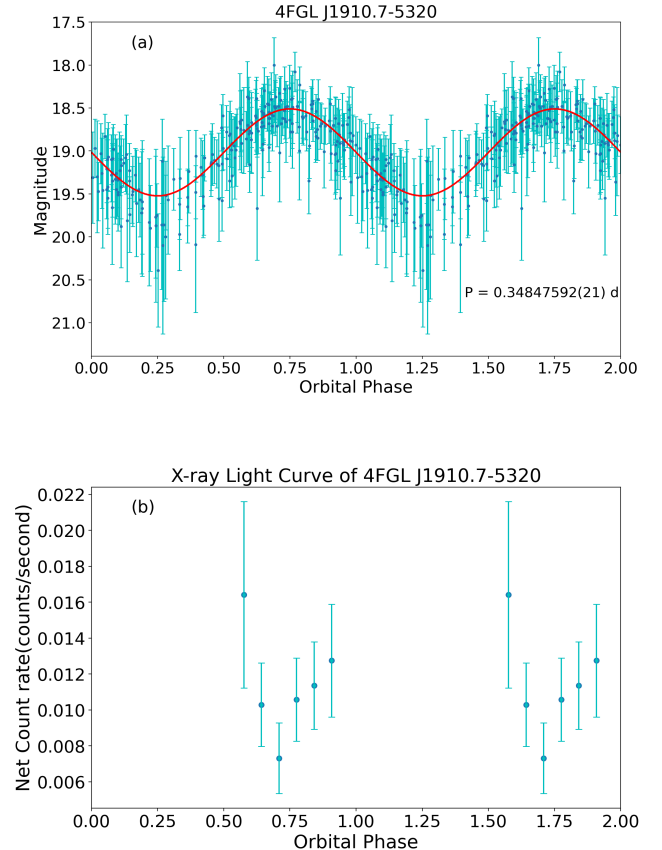


Figure 3. (a) The CRTS folded light curve and (b) the X-ray folded light curve observed by *Chandra*. The red line in (a) is the best-fit with a sinusoidal function. Both light curves are folded on the orbital period of $P = 0.34847592$ days with phase zero at BJD 2453584.0121 which is the ascending node of the pulsar.

A significant X-ray counterpart was detected at the optical position of the variable CRTS source. Its location is at R.A.(J2000) = 19^h10^m49^s.10 and Decl.(J2000) = -53°20′57″.2 with a 90% uncertainty of 0′.8. This is only 0′.17 from the CRTS variable described in §3.1, strongly suggesting that they are the same source. There are 106 source counts in a 2'' radius aperture and 164 counts in a nearby source-free circular background region with a radius of 10''. We fit the X-ray spectrum with an absorbed power-law model with the Galactic hydrogen column density of $N_H = 5.22 \times 10^{20}$ cm⁻² (fixed; Blackburn et al. 1999; HI4PI Collaboration et al. 2016)⁴. The best-fit parameters to the X-ray spectrum (Figure 5) are a photon index of $\Gamma = 1.0 \pm 0.4$ and an en-

³ <https://heasarc.gsfc.nasa.gov/xanadu/xspec>

⁴ <http://heasarc.gsfc.nasa.gov/ftools>

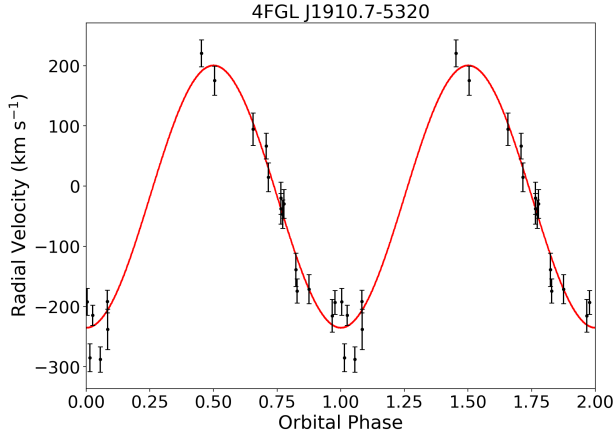


Figure 4. Radial velocity (RV) curve of 4FGL J1910.7–5320. We folded it on the orbital period of $P = 0.34847592$ days with the phase zero at BJD 2453584.0121.

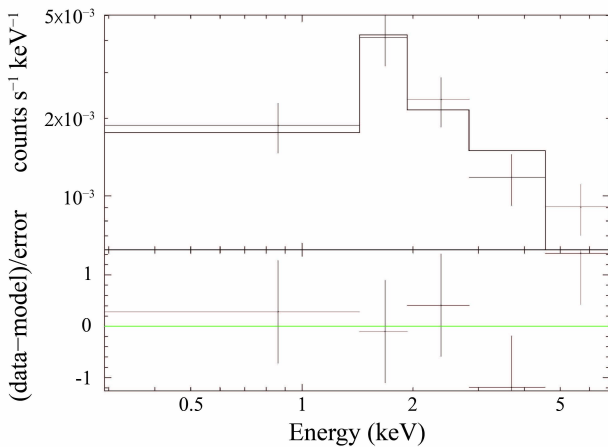


Figure 5. The X-ray spectrum in the 0.3–7 keV energy band of 4FGL J1910.7–5320. It was obtained by the best-fit power-law model.

energy flux of $F_{0.3-7\text{keV}} = (1.7 \pm 0.2) \times 10^{-13}$ erg cm $^{-2}$ s $^{-1}$ ($\chi^2/d.o.f. = 3.7/3$). The 0.3–7 keV X-ray luminosity is $L_x \lesssim (3.4 \pm 0.4) \times 10^{32}$ erg s $^{-1}$ by assuming $D \lesssim 4.1$ kpc.

We also fit the spectrum with a blackbody model, and the result is $F_{0.3-7\text{keV}} = (1.26 \pm 0.15) \times 10^{-13}$ erg cm $^{-2}$ s $^{-1}$ and a temperature of $kT = 0.9 \pm 0.1$ keV ($\chi^2/d.o.f. = 13.2/3$). The absorbed power-law model is statistically preferred by comparing the χ^2 values.

3.4. *Fermi-LAT Gamma-ray Analysis*

Here, we used Fermitools (version v11r5p3; [Fermi Science Support Development Team 2019](#)) from the *Fermi*

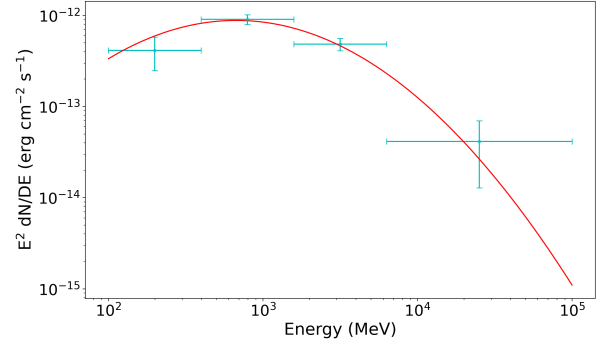


Figure 6. The γ -ray spectrum (*Fermi-LAT*; 0.1–100 GeV) of 4FGL J1910.7–5320 with the best-fit LogParabola spectral model indicated by the red line.

Science Support Center (FSSC)⁵ with the 4FGL-DR3 ([Abdollahi et al. 2022](#)) and Pass8 data (P8R3) to refine the γ -ray position and the γ -ray spectral properties of 4FGL J1910.7–5320.

We downloaded the LAT event files and spacecraft data from FSSC. The P8R3 data downloaded starts from 2008 Aug 4 to 2021 Nov 9 with energies in 0.1–300 GeV. We chose the SOURCE class events (FRONT and BACK) with a zenith angle smaller than 90° . The center of the $14^\circ \times 14^\circ$ region of interest (ROI) is at $(\alpha, \delta) = (287^\circ.705, -53^\circ.349)$, the 4FGL-DR3 position of 4FGL J1910.7–5320. We used the 4FGL-DR3 cataloged sources located within 10° from the target to establish the spatial and spectral model of the γ -ray emission. The model includes the latest Galactic interstellar (gll_iem_v07.fits) and isotropic (iso_P8R3_SOURCE_V3_v1.txt) diffuse components. We employed a LogParabola model for 4FGL J1910.7–5320 as suggested in the 4FGL-DR3, which is

$$\frac{dN}{dE} = N_0 \left(\frac{E}{E_b} \right)^{-(\alpha + \beta \log(\frac{E}{E_b}))}, \quad (2)$$

where α characterizes the photon index and β defines the degree of curvature for the LogParabola model. There is a total of 33 free parameters from the source in the emission model by allowing the background diffuse components and the sources inside a 5° radius circle from 4FGL J1910.7–5320 to vary. We performed a binned likelihood analysis with 37 logarithmically uniform energy bins, which gives test statistic (TS) value, the significance of a certain source, of 146 ($\sim 11.7\sigma$ detection significance with 3 extra parameters), a 0.1–100 GeV energy flux of $F_{0.1-100\text{GeV}} = (2.6 \pm 0.4) \times 10^{-12}$ erg cm $^{-2}$ s $^{-1}$, $\alpha = 2.2 \pm 0.2$, and $\beta = 0.3 \pm 0.2$ (Fig-

⁵ <https://fermi.gsfc.nasa.gov/ssc>

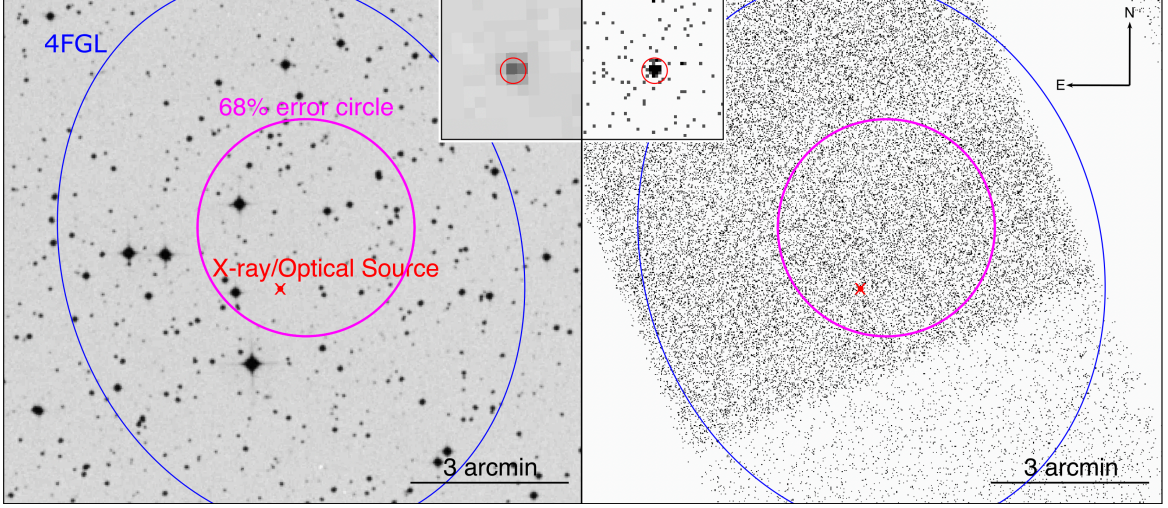


Figure 7. The Digitized Sky Survey (DSS) image (left) and the *Chandra* X-ray image (right) of 4FGL J1910.7–5320. The blue ellipses show the 95% error ellipse of 4FGL catalog. The magenta circle is the updated LAT error circle at a 68% confidence level. The small red cross is the X-ray/Optical position determined by *Chandra* (§3.3). The two upper middle inset boxes are the zoomed-in view of the optical and X-ray counterparts.

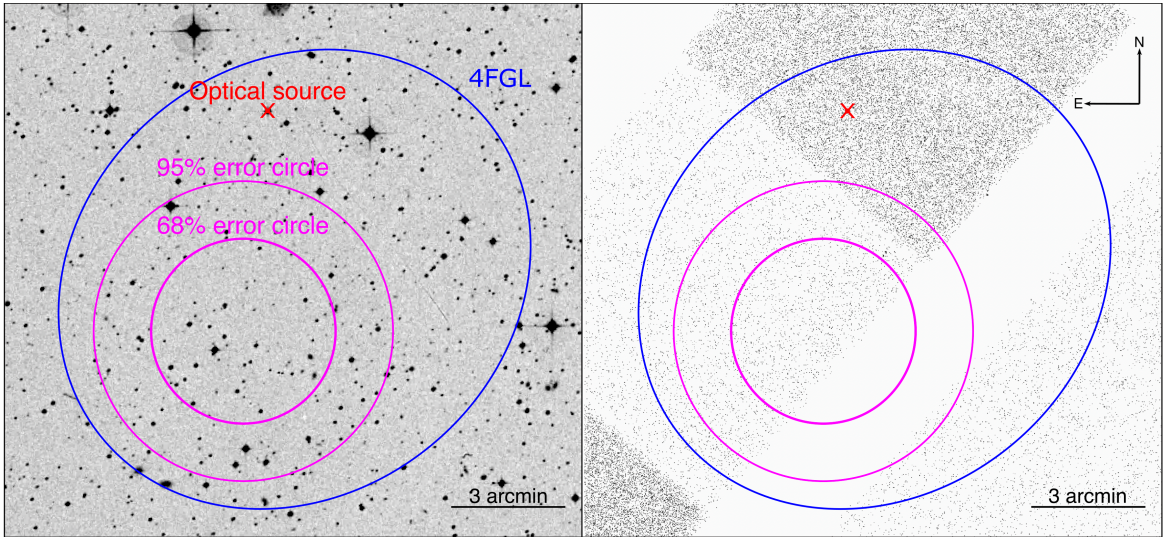


Figure 8. The DSS image (left) and the *Chandra* X-ray image (right) of 4FGL J2029.5–4237. The blue ellipses show the 95% error ellipse of the 4FGL catalog. The magenta concentric circles present the updated LAT error circles at a 68% (inside) and a 95% (outside) confidence level. The small red cross is the position determined by the CRTS survey.

ure 6). The 0.1–100 GeV γ -ray luminosity is $L_\gamma \lesssim (5.3 \pm 0.8) \times 10^{33} \text{ erg s}^{-1}$ by assuming $D \lesssim 4.1 \text{ kpc}$. Using `gtfindsrc`, we refined the 68% error circle of 4FGL J1910.7–5320 to a circular region with 2:1 radius centred at $(\alpha, \delta) = (287^\circ.691, -53^\circ.330)$ that includes the CRTS optical source (Figure 7).

4. 4FGL J2029.5–4237

The possible optical counterpart to 4FGL J2029.5–4237 is located at R.A.(J2000) = $20^{\text{h}}29^{\text{m}}34^{\text{s}}.21$ and Decl.(J2000) = $-42^\circ33'17''.6$, inside the 95% error region of the γ -ray source. Following a similar procedure

to the analysis of 4FGL J1910.7–5320, the best-fit period of the optical variable is $0.178235614(93)$ days with a mean magnitude of $14.264 \pm 0.002 \text{ mag}$ and an amplitude of $0.183 \pm 0.003 \text{ mag}$. We find no X-ray counterpart in a 11.7 ks *Chandra* observation on 2019 Sep 01, leading to a $3\text{-}\sigma$ flux upper limit of $F_{0.3\text{--}7\text{keV}} = 2.4 \times 10^{-14} \text{ erg cm}^{-2} \text{ s}^{-1}$, where we assumed the photon index to be 2 and the Galactic column density of $N_H = 3.7 \times 10^{20} \text{ cm}^{-2}$ (fixed; Blackburn et al. 1999; HI4PI Collabora-

tion et al. 2016)⁶. The corresponding 3- σ luminosity upper limit is $L_{0.3-7keV} = (3.8 \pm 0.2) \times 10^{30} \text{ erg s}^{-1}$ by assuming the *Gaia* DR3 (Gaia Collaboration 2020) distance of $D = 1.14 \pm 0.03 \text{ kpc}$.

In the *Fermi*-LAT analysis, the P8R3 data used spans from 2008 Aug 4 to 2020 Mar 25 for 4FGL J2029.5–4237. Using a LogParabola model suggested in 4FGL-DR3, the best-fit TS value is 119 (equivalent to a $> 10\sigma$ detection significance), with a 0.1–100 GeV energy flux of $F_{0.1-100GeV} = (2.0 \pm 0.2) \times 10^{-12} \text{ erg cm}^{-2} \text{ s}^{-1}$, $\alpha = 2.4 \pm 0.2$, and $\beta = 9.998$ (fixed in 4FGL-DR3, likely because it reaches the maximum limit of the parameter space). The updated 68% error circle of 4FGL J2029.5–4237 is located at $(\alpha, \delta) = (307^\circ.407, -42^\circ.651)$ with $2'4$ radius. However, the CRTS optical source is outside this improved 95% error circle (shown in Figure 8), strongly suggesting that the CRTS source is unrelated to 4FGL J2029.5–4237.

5. DISCUSSION

We find a candidate optical/X-ray counterpart to 4FGL J1910.7–5320, and the observational results strongly suggest that it is a redback MSP binary. We summarize the properties of this redback candidate below:

- An updated γ -ray 68% error circle with $2'1$ radius is presented in Figure 7 and the optical source is still inside the error circle.
- A compact orbit of $P = 8.36$ hours and $K_{2,obs} = 218 \pm 8 \text{ km s}^{-1}$, which is consistent with the orbital properties of many redbacks (Hui & Li 2019; Strader et al. 2019).
- A single peak orbital light curve of 4FGL J1910.7–5320 (Figure 3) implies that the optical emission probably is pulsar heating-dominated.
- An X-ray counterpart to the optical source is also found in *Chandra*. A hard photon index of $\Gamma = 1.0 \pm 0.4$ was shown in X-rays and the emission exhibits tentative evidence for periodic modulation.

5.1. X-ray Orbital Modulation Of 4FGL J1910.7–5320

As we mentioned in § 3.3 and Figure 3, the X-ray and optical sources probably are the counterparts to 4FGL J1910.7–5320. This association can be further confirmed, if the X-ray and optical phased light curves have any relation.

In order to explore the X-ray modulation, we folded the *Chandra* X-ray light curve on the orbital period $P = 0.34847592$ days (Figure 3). Although the observation does not cover a complete orbit, the folded light curve shows a possible dip at phase 0.75 (Figure 3). If the X-ray orbital modulation is real, it could be due to the Doppler boosting effect in the intrabinary shock (Li et al. 2014; Takata et al. 2014; Kong et al. 2017). At phase 0.75 (Figure 3), the stellar companion is behind the presumed pulsar as seen from Earth. If the momentum flux of the pulsar wind is stronger than that of the stellar wind from the companion, the intrabinary shock can wrap the companion. This means the shocked wind does not point towards Earth, and the X-ray emission therefore decreases, consistent with the *Chandra* light curve of 4FGL J1910.7–5320. Furthermore, the intrabinary shock could produce synchrotron X-ray emission that can be described by a power-law spectral model. This naturally explains the observed *Chandra* X-ray emission, which appears non-thermal with $\Gamma = 1.0 \pm 0.4$. Unfortunately, the current X-ray and optical datasets do not allow a detailed investigation. Deeper and longer observations in X-rays and the optical band (with color information) are required in the future.

5.2. 4FGL J1910.7–5320 As A Redback Or Black Widow?

From Figure 3, the optical phased light curve of 4FGL J1910.7–5320 shows an obvious one-peak signature. Since the pulsar heating effect is usually more prominent for black widows than for redbacks, this light curve feature is more consistent with that of a black widow. The optical peak and X-ray peak are shifted by half an orbit, which is similar to the original black widow PSR B1957+20 (Fruchter et al. 1988). However, there are also several black widow examples that show zero phase shift between the optical and X-ray peaks, such as PSR J1124–3653, PSR J1653–0158 and PSR J2256–1024 (Gentile et al. 2014; Long et al. 2022). Therefore, the evidence is not particularly strong to say that 4FGL J1910.7–5320 is a black widow candidate.

In §3.1, we assumed the size of the companion in the case of redback (i.e., $R \lesssim 0.7R_\odot$) and black widow (i.e., $R \lesssim 0.3R_\odot$) based on a Roche-lobe description, and estimated the distance to be $D \leq 4.1 \text{ kpc}$ and 1.8 kpc , respectively. If the system is a black widow MSP, it will be relatively close to us. In fact, the system will be much closer if it is a black widow, because the companion size of a black widow is generally smaller than the Roche-lobe radius (Draghis et al. 2019). We also performed another independent distance estimation by comparing the magnitude and the distance of 4FGL J1910.7–5320

⁶ <http://heasarc.gsfc.nasa.gov/ftools>

to the original black widow, PSR B1957+20, of which the distance is $D = 1.5\text{--}2.5$ kpc (Taylor & Cordes 1993; Cordes & Lazio 2002; van Kerkwijk et al. 2011) and the minimum optical magnitude in the R band is 24.6 mag (Reynolds et al. 2007). In 4FGL J1910.7–5320, the minimum best-fit magnitude in the CRTS catalog is 19.62 mag (~ 20.5 for the faintest data), which is about ~ 5 mag brighter than the minimum magnitude of PSR B1957+20. This implies that if 4FGL J1910.7–5320 is a black widow MSP similar to PSR B1957+20, the distance to 4FGL J1910.7–5320 is $D \sim 0.15\text{--}0.25$ kpc, which is extremely close to us. At this short distance, *Gaia* should be able to measure the parallax, and hence, the distance of 4FGL J1910.7–5320 easily. However, the parallax is not well constrained in the *Gaia* Catalog DR3 (Gaia Collaboration 2020). Therefore, interpreting 4FGL J1910.7–5320 as a reback MSP system is favored.

5.3. Strong Irradiation Signature Of 4FGL J1910.7–5320?

We notice that the irradiation signature is relatively strong (the amplitude is over 1 mag) compared to other rebacks. To check this phenomenon systematically, we used the CRTS catalog (Drake et al. 2009) to find the modulation amplitude of other known reback systems. We find that there are only two rebacks, PSR J2215+5135 (Breton et al. 2013) and PSR J2339–0533 (Romani & Shaw 2011), that have a high irradiation signature (amplitude > 1 mag) among the 14 known rebacks (Hui & Li 2019; Strader et al. 2019). A dedicated statistical study of irradiation signatures of rebacks will be published elsewhere.

5.4. 4FGL J2029.5–4237

We found a variable optical source inside the 95% error ellipse of 4FGL J2029.5–4237 and speculated that it is another MSP binary candidate. In the 11.7 ks *Chandra* observation, we found no significant X-ray source spatially coincident with the optical variable, with a $3\text{-}\sigma$ flux upper limit of 2.4×10^{-14} erg cm $^{-2}$ s $^{-1}$ (0.3–7 keV). The corresponding luminosity is $L = 3.8 \times 10^{30}$ erg s $^{-1}$ by using the *Gaia* distance of 1.14 kpc (Gaia Collaboration 2020), which is considerably lower than in many other MSPs. The optical source is also outside the updated 95% LAT error circle (Figure 8). These results strongly suggest that the variable optical source is probably not the counterpart to 4FGL J2029.5–4237 and unlikely a reback MSP.

While we were in the late stages of preparing this paper, TRAPUM discovered the radio pulsations associated with 4FGL J1910.7–5320 (i.e., PSR J1910–5320;

private communication)⁷, and confirms that 4FGL J1910.7–5320 is a reback MSP. They also found that 4FGL J2029.5–4237 is an isolated MSP, which is unrelated to the optical source reported in this paper.

⁷ <http://www.trapum.org/discoveries/>

Facilities: *Fermi*, CXO, SOAR

Software: CIAO (version 4.13; Fruscione et al. 2006), HEASOFT (Nasa High Energy Astrophysics Science Archive Research Center (Heasarc) 2014), FERMI-TOOLS (version v11r5p3; Fermi Science Support Development Team 2019)

1 The *Fermi*-LAT Collaboration acknowledges gener-
 2 ous ongoing support from a number of agencies and
 3 institutes that have supported both the development
 4 and the operation of the LAT as well as scientific data
 5 analysis. These include the National Aeronautics and
 6 Space Administration and the Department of Energy in
 7 the United States, the Commissariat à l’Energie Atom-
 8 ique and the Centre National de la Recherche Scien-
 9 tifique / Institut National de Physique Nucléaire et de
 10 Physique des Particules in France, the Agenzia Spaziale
 11 Italiana and the Istituto Nazionale di Fisica Nucleare in
 12 Italy, the Ministry of Education, Culture, Sports, Sci-
 13 ence and Technology (MEXT), High Energy Accelerator
 14 Research Organization (KEK) and Japan Aerospace
 15 Exploration Agency (JAXA) in Japan, and the K. A.
 16 Wallenberg Foundation, the Swedish Research Council
 17 and the Swedish National Space Board in Sweden. Ad-
 18 ditional support for science analysis during the opera-
 19 tions phase from the following agencies is also gratefully
 20 acknowledged: the Istituto Nazionale di Astrofisica in
 21 Italy and and the Centre National d’Etudes Spatiales in
 22 France. This work performed in part under DOE Con-
 23 tract DE-AC02-76SF00515.

24 This research has made use of data obtained from the
 25 *Chandra* Data Archive and the *Chandra* Source Cata-
 26 log, and software provided by the *Chandra* X-ray Center
 27 (CXC) in the application packages CIAO and Sherpa.

28 Based on observations obtained at the Southern As-
 29 trophysical Research (SOAR) telescope, which is a joint
 30 project of the Ministério da Ciência, Tecnologia e In-
 31 ovações (MCTI/LNA) do Brasil, the US National Sci-
 32 ence Foundation’s NOIRLab, the University of North
 33 Carolina at Chapel Hill (UNC), and Michigan State Uni-
 34 versity (MSU).

35 The CRTS survey is supported by the U.S. National
 36 Science Foundation under grants AST- 0909182 and
 37 AST-1313422.

38 KYA and KLL are supported by the National Science
 39 and Technology Council of the Republic of China (Tai-
 40 wan) through grant 111-2636-M-006-024, and KLL is
 41 also a Yushan Young Fellow supported by the Ministry
 42 of Education of the Republic of China (Taiwan).

43 JS acknowledges support by NSF grant AST-2205550
 44 and the Packard Foundation. This research was per-
 45 formed while SJS held a NRC Research Associateship
 46 award at the Naval Research Laboratory. Work at the
 47 Naval Research Laboratory is supported by NASA DPR
 48 S-15633-Y.

49 CYH is supported by the National Research Founda-
 50 tion of Korea through grants 2016R1A5A1013277 and
 51 2022R1F1A1073952.

REFERENCES

- Abdo, A., Ajello, M., Allafort, A., et al. 2013, *The Astrophysical Journal Supplement Series*, 208, 17
- Abdollahi, S., Acero, F., Ackermann, M., et al. 2020, *The Astrophysical Journal Supplement Series*, 247, 33
- Abdollahi, S., Acero, F., Baldini, L., et al. 2022, *ApJS*, 260, 53, doi: [10.3847/1538-4365/ac6751](https://doi.org/10.3847/1538-4365/ac6751)
- Alpar, M., Cheng, A., Ruderman, M., & Shaham, J. 1982, *Nature*, 300, 728
- Archibald, A. M., Stairs, I. H., Ransom, S. M., et al. 2009, *Science*, 324, 1411
- Arnaud, K. 1996, in *Astronomical Data Analysis Software and Systems V*, Vol. 101, 17
- Atwood, W., Abdo, A. A., Ackermann, M., et al. 2009, *The Astrophysical Journal*, 697, 1071
- Bailer-Jones, C., Rybizki, J., Fouesneau, M., Demleitner, M., & Andrae, R. 2021, *The Astronomical Journal*, 161, 147
- Bellm, E. C., Kulkarni, S. R., Graham, M. J., et al. 2018, *Publications of the Astronomical Society of the Pacific*, 131, 018002
- Bianchi, L., Herald, J., Efremova, B., et al. 2011, *Astrophysics and Space Science*, 335, 161
- Blackburn, J., Shaw, R., Payne, H., Hayes, J., et al. 1999, *Astrophysics Source Code Library*, ascl
- Breton, R., Van Kerkwijk, M., Roberts, M., et al. 2013, *The Astrophysical Journal*, 769, 108
- Brown, A., Vallenari, A., Prusti, T., et al. 2018, *Astronomy & astrophysics*, 616, A1
- Burdge, K. B., Marsh, T. R., Fuller, J., et al. 2022, *Nature*, 605, 41
- Cardelli, J. A., Clayton, G. C., & Mathis, J. S. 1989, *The Astrophysical Journal*, 345, 245
- Chen, H.-L., Chen, X., Tauris, T. M., & Han, Z. 2013, *The Astrophysical Journal*, 775, 27
- Clemens, J. C., Crain, J. A., & Anderson, R. 2004, in *Ground-based Instrumentation for Astronomy*, Vol. 5492, SPIE, 331–340
- Cordes, J. M., & Lazio, T. J. W. 2002, arXiv preprint [astro-ph/0207156](https://arxiv.org/abs/astro-ph/0207156)
- Draghis, P., Romani, R. W., Filippenko, A. V., et al. 2019, *The Astrophysical Journal*, 883, 108
- Drake, A., Djorgovski, S., Mahabal, A., et al. 2009, *The Astrophysical Journal*, 696, 870
- Drake, A., Djorgovski, S., Catelan, M., et al. 2017, *Monthly Notices of the Royal Astronomical Society*, 469, 3688
- Eggleton, P. P. 1983, *The Astrophysical Journal*, 268, 368
- Fermi Science Support Development Team. 2019, *Fermitools: Fermi Science Tools*, Astrophysics Source Code Library, record ascl:1905.011. <http://ascl.net/1905.011>
- Fruchter, A., Stinebring, D., & Taylor, J. 1988, *Nature*, 333, 237
- Fruscione, A., McDowell, J. C., Allen, G. E., et al. 2006, in *Observatory Operations: Strategies, Processes, and Systems*, Vol. 6270, International Society for Optics and Photonics, 62701V
- Gaia Collaboration. 2020, *VizieR Online Data Catalog*, I/350
- Gaia Collaboration, Prusti, T., de Bruijne, J. H. J., et al. 2016, *A&A*, 595, A1, doi: [10.1051/0004-6361/201629272](https://doi.org/10.1051/0004-6361/201629272)
- Gentile, P., Roberts, M., McLaughlin, M., et al. 2014, *The Astrophysical Journal*, 783, 69
- HI4PI Collaboration, Ben Bekhti, N., Flöer, L., et al. 2016, *A&A*, 594, A116, doi: [10.1051/0004-6361/201629178](https://doi.org/10.1051/0004-6361/201629178)
- Hui, C., Wu, K., Han, Q., Kong, A., & Tam, P. 2018, *The Astrophysical Journal*, 864, 30
- Hui, C., Park, S., Hu, C., et al. 2015, *The Astrophysical Journal*, 809, 68
- Hui, C. Y., & Li, K. L. 2019, *Galaxies*, 7, 93
- Kong, A., Hui, C., Takata, J., Li, K., & Tam, P. 2017, *The Astrophysical Journal*, 839, 130
- Kong, A. K., Jin, R., Yen, T.-C., et al. 2014, *The Astrophysical Journal Letters*, 794, L22
- Lasker, B. M., Lattanzi, M. G., McLean, B. J., et al. 2008, *The Astronomical Journal*, 136, 735
- Li, K., Kong, A., Takata, J., et al. 2014, *The Astrophysical Journal*, 797, 111
- Li, K.-L., Kong, A. K., Hou, X., et al. 2016, *The Astrophysical Journal*, 833, 143
- Li, K.-L., Hou, X., Strader, J., et al. 2018, *The Astrophysical Journal*, 863, 194
- Long, J. S., Kong, A. K., Wu, K., et al. 2022, *The Astrophysical Journal*, 934, 17
- Marocco, F., Eisenhardt, P. R., Fowler, J. W., et al. 2021, *The Astrophysical Journal Supplement Series*, 253, 8
- McMahon, R. G., Banerji, M., Gonzalez, E., et al. 2013, *The Messenger*, 154, 188
- Moss, A., von Hippel, T., Robinson, E., et al. 2022, *The Astrophysical Journal*, 929, 26
- Nasa High Energy Astrophysics Science Archive Research Center (Heasarc). 2014, *HEASoft: Unified Release of FTOOLS and XANADU*, Astrophysics Source Code Library, record ascl:1408.004. <http://ascl.net/1408.004>
- Papitto, A., Ferrigno, C., Bozzo, E., et al. 2013, *Nature*, 501, 517

- Patruno, A., Archibald, A., Hessels, J., et al. 2013, *The Astrophysical Journal Letters*, 781, L3
- Reynolds, M. T., Callanan, P. J., Fruchter, A. S., et al. 2007, *Monthly Notices of the Royal Astronomical Society*, 379, 1117
- Roberts, M. S. E. 2011, in *American Institute of Physics Conference Series*, Vol. 1357, *Radio Pulsars: An Astrophysical Key to Unlock the Secrets of the Universe*, ed. M. Burgay, N. D'Amico, P. Esposito, A. Pellizzoni, & A. Possenti, 127–130, doi: [10.1063/1.3615095](https://doi.org/10.1063/1.3615095)
- Romani, R. W., & Sanchez, N. 2016, *ApJ*, 828, 7, doi: [10.3847/0004-637X/828/1/7](https://doi.org/10.3847/0004-637X/828/1/7)
- Romani, R. W., & Shaw, M. S. 2011, *The Astrophysical Journal Letters*, 743, L26
- Roy, J., Ray, P. S., Bhattacharyya, B., et al. 2015, *The Astrophysical Journal Letters*, 800, L12
- Schlegel, D. J., Finkbeiner, D. P., & Davis, M. 1998, *The Astrophysical Journal*, 500, 525
- Stappers, B., Archibald, A., Hessels, J., et al. 2014, *The Astrophysical Journal*, 790, 39
- Strader, J., Li, K.-L., Chomiuk, L., et al. 2016, *The Astrophysical Journal*, 831, 89
- Strader, J., Swihart, S., Chomiuk, L., et al. 2019, *The Astrophysical Journal*, 872, 42
- Swihart, S. J., Strader, J., Aydi, E., et al. 2022, *ApJ*, 926, 201, doi: [10.3847/1538-4357/ac4ae4](https://doi.org/10.3847/1538-4357/ac4ae4)
- Takata, J., Li, K., Leung, G. C., et al. 2014, *The Astrophysical Journal*, 785, 131
- Tauris, T. M. 2011, 447, 285, <https://arxiv.org/abs/1106.0897>
- Taylor, J. H., & Cordes, J. M. 1993, *ApJ*, 411, 674, doi: [10.1086/172870](https://doi.org/10.1086/172870)
- Tody, D. 1986, in *Instrumentation in astronomy VI*, Vol. 627, SPIE, 733–748
- Van den Heuvel, E., & Van Paradijs, J. 1988, *Nature*, 334, 227
- van Kerkwijk, M. H., Breton, R. P., & Kulkarni, S. R. 2011, *ApJ*, 728, 95, doi: [10.1088/0004-637X/728/2/95](https://doi.org/10.1088/0004-637X/728/2/95)
- Weisskopf, M., Brinkman, B., Canizares, C., et al. 2002, *Publications of the Astronomical Society of the Pacific*, 114, 1
- Yap, Y. X., Li, K. L., Kong, A. K. H., et al. 2019, *A&A*, 621, L9, doi: [10.1051/0004-6361/201834545](https://doi.org/10.1051/0004-6361/201834545)